LARGE EDDY SIMULATION OF AN ANNULAR SWIRLING JET WITH PULSATING INFLOW

Manuel García-Villalba, Jochen Fröhlich and Wolfgang Rodi
SFB 606, University of Karlsruhe,
76128 Karlsruhe, Germany
villalba@ifh.uka.de, froehlich@ict.uni-karlsruhe.de,
rodi@ifh.uni-karlsruhe.de

ABSTRACT

The effect of oscillating inflow on an annular swirling jet is studied by means of large eddy simulation and the results obtained are compared to the same configuration with constant inflow. To assess the influence of the swirl generation method used in applications, two extreme cases are considered, one with pulsating axial and tangential velocity component, one with pulsating axial component only. In both cases the phase-averaged flow features vortex rings. When the phase-averaged flow is removed, instantaneous coherent structures are observed which resemble those of the non-pulsating case. Their coherence is higher when only the axial component oscillates. Analysis of phase-averaged velocity components, vorticity, turbulent kinetic energy and spectra provides detailed information about the flows considered.

INTRODUCTION

In many combustion devices, a swirling flow is used to stabilize the flame through a recirculation zone. Swirling flows, however, are prone to instabilities which can trigger combustion oscillations and degrade the performance of the device. In the case of a thermo-acoustic combustion instability, temporal oscillations of the pressure in the combustion chamber induce substantial fluctuations of the mass flow rate into the combustion chamber at the burner outlet. It is therefore of crucial importance to investigate the effect of a pulsating flow rate in the presence of swirl. For non-swirling pulsating jets, experiments and simulations (Tang and Ko, 1994, Wicker and Eaton, 1994)) have shown dominant ring vortices.

Combustor flows are characterized by high Reynolds numbers and therefore broadband turbulence. Numerical simulations, in particular Large Eddy Simulations (LES), often provide more detailed information than experiments because full instantaneous three-dimensional fields are available and a deeper understanding of the flow physics can be achieved. Recently, due to the increase in computing power, LES of swirling flows have started to appear in the literature (Apte *et al.* 2003, Wang *et al.* 2004, Wegner *et al.* 2004, Lu *et al.* 2005) following the pioneering work of Pierce and Moin (1998*b*). In this context only few attempts have been made so far to compute and analyze swirling flows with pulsating inflow. Düsing *et al.* (2002) performed LES of a swirling confined diffusion flame with oscillating inflow. The averaging time, however, was not long enough to obtain definite conclusions. Wang *et al.* (2003) studied the flow evolution of a swirl-stabilized injector and its dynamic response to external forcing using LES. In this case, the configuration was very complex, however, involving three radial swirlers, with the flow in one of them counter-rotating with respect to the others. Furthermore, the forcing was weak with respect to the flow intensity, and had only a small impact on the flow characteristics.

In García-Villalba *et al.*(2004*b*, 2005) the present authors performed LES of an unconfined annular swirling jet. Large-scale coherent helical structures precessing around the symmetry axis at a constant rate were identified by means of visualizations and temporal spectra. The purpose of the present paper is to study the influence of an imposed oscillating inflow on the previously observed large-scale coherent structures in the presence of substantial swirl.

NUMERICAL SETUP

The flow configuration was set up according to the experiments performed at the University of Karlsruhe (Hillemanns, 1988) and is shown together with the calculation domain in Fig.1. The Reynolds number of the non-pulsating flow based on the bulk velocity U_b and the jet diameter D is $Re = 163000$. The swirl parameter is $S = 1.2$ defined at the inflow plane $x/D = -1$ as

$$S = \frac{\int_0^R \int_0^{2\pi} \rho\, u_x\, u_\theta\, r^2\, d\theta\, dr}{R \int_0^R \int_0^{2\pi} \rho\, u_x^2\, r\, d\theta\, dr}, \qquad (1)$$

where u_x and u_θ are the axial and azimuthal velocity component, respectively, and $R = D/2$ is the outer radius of the annular jet.

The simulations were performed with the code LESOCC2 (Hinterberger, 2004), using a second-order accurate finite volume method. The curvilinear block-structured mesh consists of about 6 million cells. No-slip boundary conditions were applied at the walls. The entrainment was simulated using a mild co-flow of $0.05U_b$ and free-slip conditions were applied at the open lateral boundary located far away from the region of interest (see Fig.1). A convective outflow condition was used at the exit boundary. The inflow conditions were obtained by performing simultaneously a separate, periodic LES of swirling flow in an annular pipe using body forces to impose swirl number and flow rate as described in Pierce and Moin (1998*a*). The dynamic subgrid-scale model was employed with smoothing by temporal relaxation. This approach has been previously applied and successfully validated for the present configuration in García-Villalba *et al.*(2004*a*).

The pulsating inflow was prescribed by imposing an pulsating flow rate in the precursor simulation according to

$$Q = Q_0 \left(1 + B\, \sin\left(\frac{2\pi t}{T}\right)\right), \qquad (2)$$

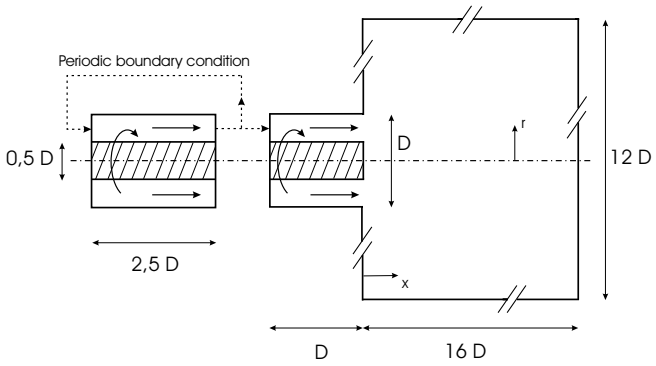

Figure 1: Computational domain and generation of inflow data. Note that the boundaries in the right part are not displayed to scale.

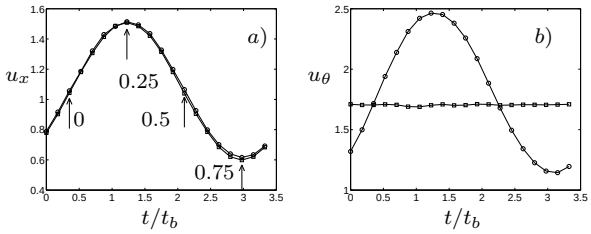

Figure 2: Phase-averaged velocity at the inflow plane $x/R = -2$ at $r/R = 0.75$, i.e. in the middle of the annular duct, as a function of time over one period. *a*) Axial component $\widetilde{u_x}/U_b$ and phases discussed below. *b*) Tangential component $\widetilde{u_\theta}/U_b$. Sim.2: circles. Sim.3: squares.

where Q_0 is the flow rate without pulsation. The amplitude of the disturbance is $B = 0.4$ in the present configuration which corresponds to experimentally observed values. The oscillation period was set to $T = 3.5R/U_b$ which roughly equals the precessing period of the coherent structures observed in the non-pulsating simulations (García-Villalba *et al.*, 2004*b*) and is also motivated by experimental data from thermo-acoustic instabilities (Büchner, 2005).

Table 1 provides an overview over the simulations performed. Two cases have been considered depending on the specification of the inflow conditions. In Sim.2, the mass flow oscillates periodically while the swirl number is kept fixed so that both, the axial and the azimuthal velocity component oscillate periodically (see equations (1),(2) and Fig.2). In Sim.3, the body force in the azimuthal direction is kept constant while only the axial flow rate pulsates, Fig.2. As a consequence, the swirl number oscillates. Note that different scenarios of pulsation are realistic since the swirl-generating devices in a burner can be different. An axial swirl generator with helical vanes maintains the angle of the flow so that the swirl number will change only little as in Sim.2. With a radial swirler, on the other hand, the axial component can be influenced independently of the angular component upon the occurrence of a thermo-acoustic instability resulting in an oscillating flow angle and an oscillating swirl number. Hence, the two cases considered in the present work are representative of extreme cases in applications and allow to assess the sensitivity of the observations with respect to the method of swirl generation. Finally, Sim.1 is the reference case without pulsation from García-Villalba *et al.*, (2004*b*).

Table 1: Overview over the simulations

Simulation	B	TU_b/R	Mass flow	Swirl number
1	-	-	Fixed	Fixed
2	0.4	3.5	Oscillating	Fixed
3	0.4	3.5	Oscillating	Oscillating

PHASE-AVERAGED FLOW

In order to analyze the flow, each quantity ϕ can be decomposed as

$$\phi = \widetilde{\phi} + \phi'' \quad , \tag{3}$$

where $\widetilde{\phi}$ denotes the phase average. The phase itself is defined as

$$\psi = \mathrm{mod}\left(\frac{t}{T}, 1\right) \quad . \tag{4}$$

With equation (2) this implies that $Q(\psi = 0) = Q_0$ while for $\psi = 0.25$ and $\psi = 0.75$ the flow rate is maximal and minimal, respectively. All averaged quantities given below are the resolved ones.

After the computation of several periods, the phase-averaged statistics were gathered during 15 periods of pulsation and averaging was also performed in azimuthal direction. Each period was divided into 20 phases and the four phases displayed in Fig.2*a* are selected for discussion here. Figs. 3-5 show velocity profiles from the three simulations at two axial stations in the near field of the jet exit. Further profiles are not shown here due to the limited space. The influence of the pulsation decreases with distance from the jet exit. The most important characteristics of the simulation without pulsation, Sim.1, are a recirculation zone, typical for flows with a high level of swirl (Gupta *et al.*,1984) and two shear layers, an inner one bordering the recirculation zone and an outer one between the jet and the surrounding co-flow. Due to the swirl, both shear layers are three-dimensional and subject to curvature effects.

The impact of the pulsating inflow on the recirculation zone can be observed in Fig.3$c-f$ displaying phase-averaged axial velocity profiles, $\widetilde{u_x}(\psi)$. In Sim.3, the shape of the recirculation zone is almost unaffected by the pulsation as revealed by comparison of Fig.3*b* and Fig.3*f* for $r/R < 0.5$. In Sim.2, the backflow region widens with the deceleration of the flow indicating that the recirculation zone is affected by the oscillation of the azimuthal component. The influence of the pulsation on the shear layers is more difficult to quantify because it involves both axial and tangential velocity components. The latter is shown in Fig.4. As expected, the tangential profile changes substantially in Sim.2 at $x/R = 0.1$. This is not only related to a change in amplitude but also a substantial change in shape and affects mainly the inner shear layer. Further downstream, the phase-averaged tangential component also oscillates in the outer part of the jet (Fig.4*d*). With fixed tangential forcing in Sim.3, the inter-phase changes in the inner part are very small, but in the outer part, $r > R$, say, they attain amplitudes comparable to Sim.2. Comparing results at $x/D = 0.1$ and $x/R = 1$, a time lag between the flow at the inlet and the tangential component downstream of the inlet is observed. When the flow at the inlet starts to accelerate (shortly after $\psi = 0.75$) the tangential component attains its maximum in both Sim.2 and Sim.3, although the effect is better seen in Sim.2. During the acceleration phase ($\psi = 0.75 \rightarrow 0.25$), the tangential profile spreads radially outwards.

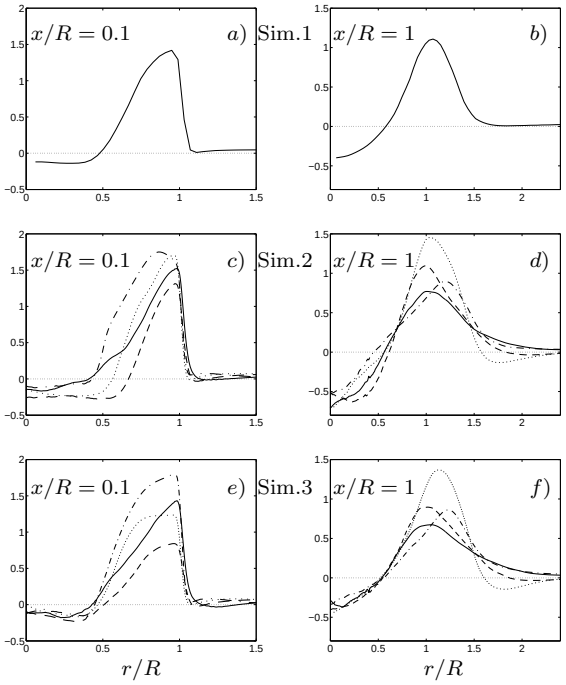

Figure 3: Radial profiles of axial velocity u_x/U_b at $x/R = 0.1$ (left) and $x/R = 1$ (right). $a-b$) Time-averaged velocity in Sim.1. $c-d$) Phase-averaged velocity in Sim.2. $e-f$) Phase-averaged velocity in Sim.3. Phases as indicated in Fig.2. Key to lines is given in Table 2.

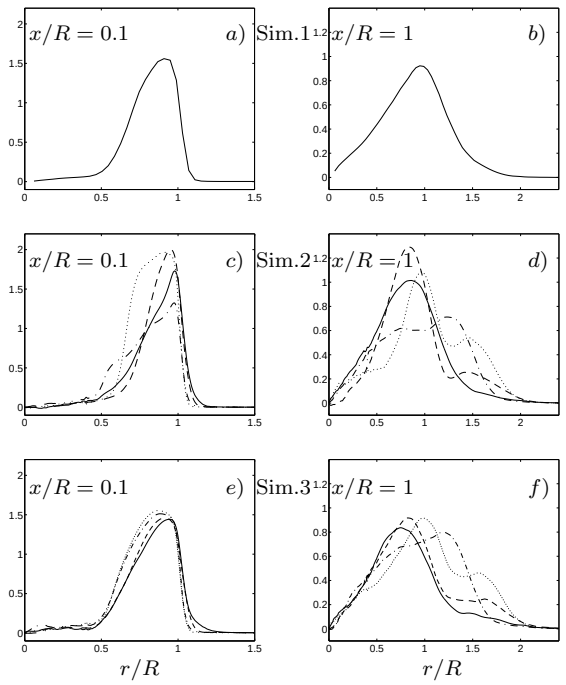

Figure 4: Profiles of tangential velocity u_θ/U_b at $x/R = 0.1$ (left) and $x/R = 1$ (right). $a-b$) Time-averaged velocity in Sim.1. $c-d$) Phase-averaged velocity in Sim.2. $e-f$) Phase-averaged velocity in Sim.3 Phases as indicated in Fig.2. Key to lines is given in Table 2.

In the simulation without pulsating inflow, the radial velocity component, shown in Fig.5, is very small compared to the other two components. In the pulsating cases, however, it exhibits substantial variations. At $x/R = 1$, it varies between $\widetilde{u_r}(0.75) \sim -0.4$ and $\widetilde{u_r}(0.25) \sim 0.4$ in Sim.2, and similar values occur in Sim.3. This is related to the roll-up of the outer shear layer, in which a ring vortex is produced. Fig.6 shows a series of contour plots of phase-averaged tangential vorticity $\widetilde{\omega_\theta}$. Its behaviour is very similar in both simulations. When the flow accelerates at the inlet ($\psi = 0.75 \rightarrow 0.25$) the sheet of negative azimuthal vorticity moves radially outwards and during the deceleration proccess ($\psi = 0.25 \rightarrow 0.75$) the ring vortex is shed.

Fig.7 reports contour plots of the turbulent kinetic energy k. In the non-pulsating simulation it is defined by the fluctuations with respect to the time average. In this case the kinetic energy is concentrated in the two shear layers of which the inner one extends substantially into the inlet duct. The maximum is about $k/U_b^2 = 0.3$ and k rapidly decays with distance from the jet exit. At $x/R > 3$ k/U_b^2 is smaller than 0.1. In the simulations with oscillating inflow, k is defined by means of the fluctuations with respect to the phase average. Again, most of this kinetic energy is concentrated in the shear layers. In both Sim.2 and Sim.3 the turbulent fluctuations in the outer part are observed at the locations of the vortex ring discussed above, as revealed by comparing corresponding plots in Fig.6 and Fig.7. During the phases $\psi = 0$ and $\psi = 0.25$, to a smaller extent also for $\psi = 0.5$, an accumulation of kinetic energy is visible further downstream, moving towards the axis which results from the vortex ring shed during the previous period. The main differences between Sim.2 and Sim.3 are noticed in the inner shear layer. In Sim.2, the kinetic energy in the inner part oscillates with the flow. In the acceleration phase ($\psi = 0.75 \rightarrow 0.25$) the kinetic energy is substantially reduced in this region, re-appearing in the inlet duct during the deceleration phase ($\psi = 0.25 \rightarrow 0.75$). In Sim3, the overall level of k is higher. An accumulation of kinetic energy in the region of the inner shear layer is observed in all phases. It remains at this location and is only little affected by the pulsation, except for the intensification and elongation during the deceleration phase, i.e. for $\psi = 0.5$. These observations are in line with the discussion of the profiles of phase-averaged velocity components above.

Table 2: Key to lines

Phase ψ	0	0.25	0.5	0.75
Line	———	—·—	·····	– – –

INSTANTANEOUS STRUCTURES

In order to visualize instantaneous coherent structures, isosurfaces of the instantaneous pressure deviation $p'' = p - \widetilde{p}$ are reproduced in Fig.8. To enhance visibility, the pressure was filtered by applying twice a top hat filter of width equal to twice the grid spacing. In Sim.1 large-scale coherent structures rotating at a constant rate around the symmetry axis can be identified (Fig.8a). It was shown in García-Villalba *et al.*(2004b) that two families of structures appear. The outer structures are located in the outer shear layer where

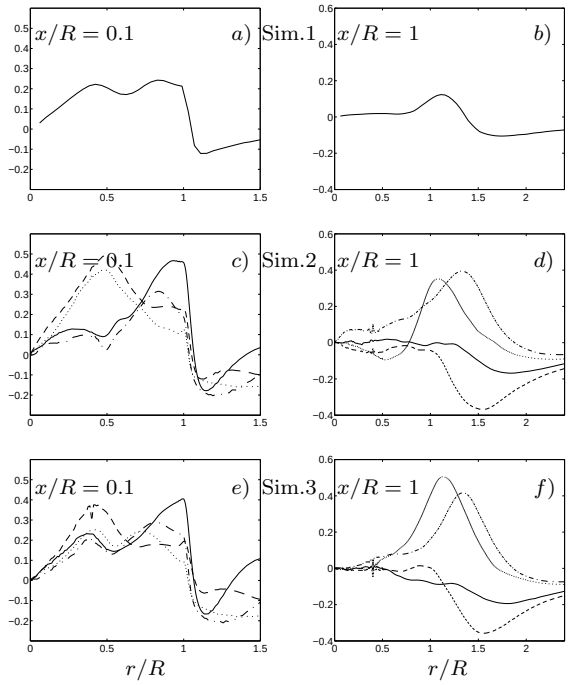

Figure 5: Profiles of average radial velocity u_r/U_b at $x/R = 0.1$ (left) and $x/R = 1$ (right). $a - b$) Time-averaged velocity in Sim.1. $c - d$) Phase-averaged velocity in Sim.2. $e - f$) Phase-averaged velocity in Sim.3 Phases as indicated in Fig.2. Key to lines is given in Table 2.

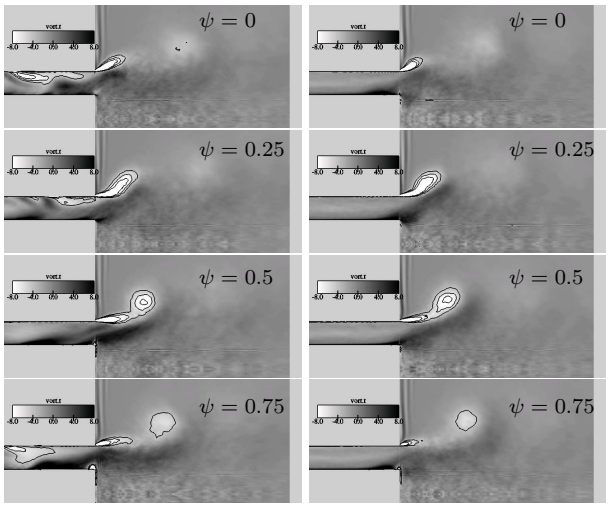

Figure 6: Phased-averaged tangential vorticity $\widetilde{\omega_\theta}$ in a plane $\theta = const.$

$\partial\langle u_x\rangle/\partial r < 0$, while the darker structures in the inner shear layer prevail where $\partial\langle u_x\rangle/\partial r > 0$. In the cited reference it was shown that these structures result from Kelvin-Helmholtz instabilities. Furthemore, the constant rate of rotation leads to pronounced energy peaks in the frequency spectra of the velocity fluctuations. The power spectral density (PSD) of axial velocity fluctuations of this case is shown in Fig.9a by a solid line. Similar peaks appear for the other components.

The influence of the oscillating inflow on the coherent structures is illustrated in Fig.8$b - c$. For conciseness, only one snapshot is included here for each simulation, but further views and animations were produced upon which the following comments are based. As in the case without pulsation, coherent structures located in both shear layers are visible. In Sim.2, Fig.8b, the structures are less organized and persist during shorter times. In Sim.3, Fig.8c, the structures resemble those of Sim.1, both in shape and regularity. Here, the pulsation has more impact on the outer structures than on the inner ones. Due to the successive processes of acceleration and deceleration, the outer structures are subject to stretching. Thus, secondary instabilities oriented in streamwise direction are formed to a larger extent than in the non-pulsating case. Two of these structures can, e.g., be seen at the outer boundary of the outer spiral in Fig.8c.

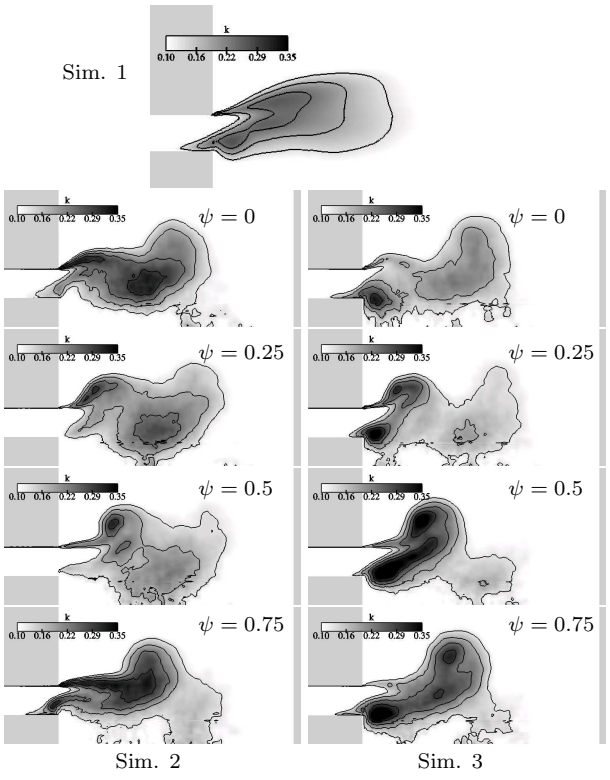

Figure 7: Turbulent kinetic energy k/U_b^2 contour plots in a plane $\theta = const.$ Top 1: Sim.1. Left: Sim.2, Right: Sim.3.

The visualization technique used in Fig.8 requires some discussion. In previous studies such as Fröhlich *et al.*(2005), e.g., it was found advantageous to use pressure fluctuations instead of the instantaneous pressure itself to identify vortices: subtracting the average pressure helps in assuring that the chosen pressure level visualizes vortex structures in a wider range of the domain. The average pressure field is not related to turbulent structures and can hence be subtraced without problem. Here, in contrast, the phase-averaged pressure is subtracted in Fig.8$b - c$ which by itself may contain dynamic structures. In the present case these have the form of the rings as discussed above. For validation and comparison, iso-surfaces of the pressure have been generated for the same data sets and are reported as well. Their behaviour is similar, showing that the vortex rings generated by the pulsation do not overwhelm the swirl-generated structures in the flows considered. Iso-surfaces of p'' are not closed here and allow better iden-

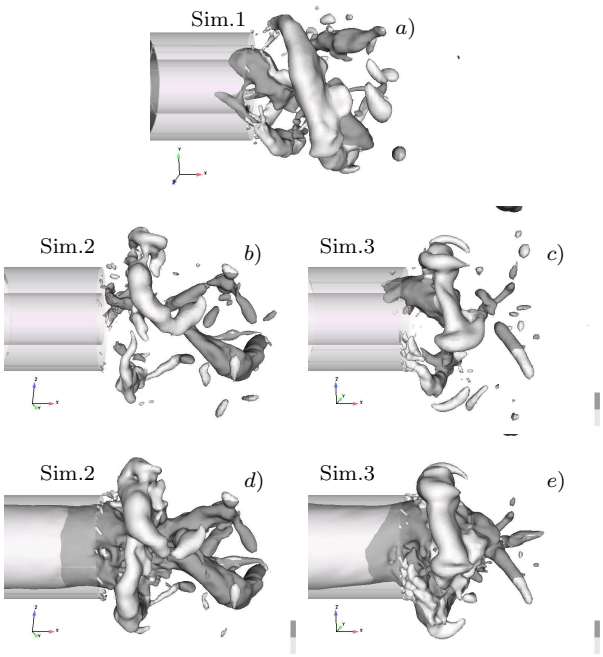

Figure 8: Instantaneous coherent structures at $\psi = 0.25$ (arbitrary phase with Sim.1). $a-c$) Iso-surface $p'' = -0.3$, $d-e$) Iso-surface $p = -0.5$ for the same data sets. The color is determined by the sign of the radial gradient of the phase-averaged axial velocity (in Sim.1 the time-average).

tification of the structures. Application of this technique in general cases, however, is not warranted without preliminary validation.

The previous observations of instantaneous structures are confirmed by analyses of the power spectral density of the velocity fluctuations. To compute the PSD, the phase-averaged velocities have been removed from the signals. Fig.9*a* presents a comparison between the three cases at $x/R = 0.1$, $r/R = 0.6$, i.e. in the inner shear layer. The pronounced peaks which are observed in Sim.1, are also present in Sim.3 while they do not occur in Sim.2. First of all, Fig.8*b* shows that the inner structures in Sim.2 are substantially weaker and more distorted which would reduce the intensity of corresponding peaks in the spectrum. Second, the rotation rate of the structures is not constant in time since the angular velocity pulsates, so that a pronounced peak cannot be expected. In Sim.3 the tangential velocity is roughly constant at the inlet. Therefore the coherent structures rotate at a constant rate as in the case without pulsation, generating pronounced peaks in the spectrum. These are even somewhat stronger than with Sim.1.

Fig.9*b* presents a comparison of the PSD of radial velocity fluctuations between the three cases at $x/R = 0.9$, $r/R = 1.2$, i.e. in the outer shear layer. In Sim.1, the regularity of the outer structures in Fig.8*a* produces a pronounced peak in the spectrum. This is not the case for the pulsating simulations. Note that the vortex rings of the phase-averaged flow do not influence these spectra, because the phase-averaged signals have been removed to compute the PSD. This figure demonstrates that the outer structures in Sim.3 (Fig.8*c*) are substantially less regular than those of Sim.1.

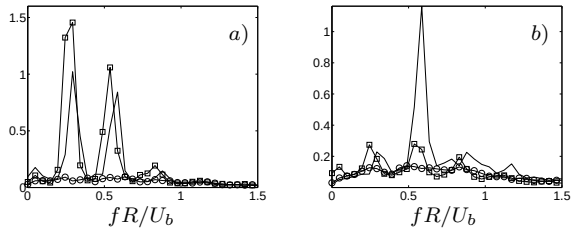

Figure 9: PSD of velocity fluctuations. *a*) PSD of axial velocity fluctuations at $x/R = 0.1$, $r/R = 0.6$. *b*) PSD of radial velocity fluctuations at $x/R = 0.9$, $r/R = 1.2$. Solid line: Sim.1, circles: Sim.2, squares: Sim.3. Arbitrary units are used in the vertical axis.

ANISOTROPY OF THE FLOW

In order to characterize the local state of the Reynolds-stress anisotropy,

$$b_{ij} = \frac{\widetilde{(u_i'' u_j'')}}{\widetilde{(u_k'' u_k'')}} - \frac{1}{3}\delta_{ij}, \tag{5}$$

the second and third invariant $II = -b_{ij}b_{ij}/2$, $III = b_{ij}b_{jk}b_{ki}/3$ are computed and assembled in the so-called "flatness parameter" or "anisotropy index" introduced by Lumley (1978),

$$A = 1 + 9(3III + II) \quad . \tag{6}$$

This parameter is useful because in isotropic turbulence both invariants vanish and $A = 1$ while for one-component and two-component turbulence $A = 0$.

Fig.10 shows radial profiles of the anisotropy index A at the same locations as the phase-averaged flow discussed above, Figs. 3-5. In the simulation without oscillating inflow, Fig.10$a-b$, the largest deviations from isotropy take place in the regions where the coherent structures are present. This happens at $x/R = 0.1$, Fig.10*a*, in the inner shear layer roughly between $r/R = 0.6$ and $r/R = 0.9$, and at $x/R = 1$, Fig.10*b*, in the outer shear layer roughly between $r/R = 1$ and $r/R = 1.4$. In Sim.3 with pulsating inflow, A is almost unaffected by the pulsation in the inner region (compare Fig.10*e* and Fig.10*a*) while in Sim.2, Fig.10*c*, a change in shape is observed. This is related to the fact that the inner structures are similar in Sim.1 and Sim.3, rotating at a constant rate, while they are weaker and non-regular in Sim.2. In the outer region, the anisotropy varies with phase for both simulations. In Sim.3, Fig.10f, for example, the largest deviation of isotropy occurs at $r/R = 1.5$ when $\psi = 0.25$ and at $r/R = 0.9$ when $\psi = 0.5$, while similar values occur in Sim.2, Fig.10*d*. This suggests, as already revealed by the spectra in Fig.9*b*, that the behaviour of the outer structures is affected by the pulsation while the inner structures are similar for Sim.1 and Sim.3.

CONCLUSIONS

Large eddy simulations of an annular swirling jet with and without pulsating inflow have been performed. The recirculation zone is mainly influenced by the oscillation of azimuthal velocity. In both cases, vortex rings are observed in the phase-averaged flow. The turbulent kinetic energy is concentrated in the shear layers. The rotation rate of the instantaneous

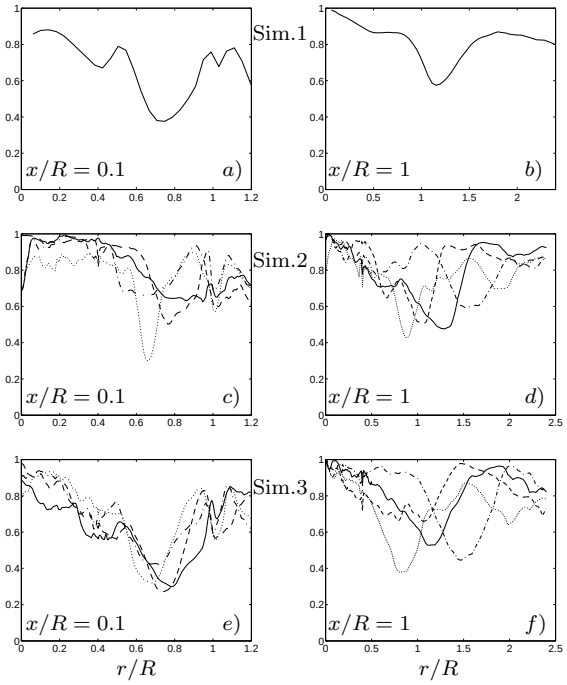

Figure 10: Anisotropy index A as a function of r/R at $x/R = 0.1$ and $x/R = 1$. $a - b$) Sim.1. $c - d$) Sim.2. $e - f$) Sim.3. Phases as indicated in Fig.2. Key to lines is given in Table 2.

coherent structures is dominated by the oscillation of the azimuthal component. When the latter is fixed at the inlet, the structures rotate at a constant rate and pronounced peaks are observed in the spectra. When the flow oscillates azimuthally at the inlet, temporal spectra cannot be used to assess spatial structures. Analyses of the instantaneous pressure field show that the qualitative nature of the vortex structures is similar to that in the non-pulsating case. The coherence of the structures, in particular for the inner ones, is larger when only the axial velocity component oscillates.

ACKNOWLEDGEMENTS

The authors acknowledge gratefully the support of the German Research Foundation (DFG) through the Collaborative Research Center SFB 606 'Unsteady Combustion'. The calculations were carried out on the IBM Regatta of the Computing Centre in Garching, and the assistance of Dr. I. Weidl is gratefully acknowledged.

REFERENCES

Apte, S.V., Mahesh, K., Moin, P. and Oefelein, J.C. 2003 "Large-eddy simulation of particle-laden flows in a coaxial-jet combustor". *Int. J. Multiphase Flow* **29**, pp. 1311–1331.

Büchner, H. 2005. Private communication.

Düsing, M., Hauser, A., Sadiki, A. and Janicka, J. 2002 "LES of confined methane-air diffusion flames using oscillation inflow conditions". In *Engineering Turbulence Modelling and Experiments 5* (eds. W. Rodi and N. Fueyo), Elsevier, pp. 917–926.

Fröhlich, J., Mellen, C.P., Rodi, W., Temmerman, L. and Leschziner, M.A. 2005 "Highly resolved large-eddy simulation of separated flow in a channel with streamwise periodic constrictions". *J. Fluid Mech.* **526**, pp. 19–66.

García-Villalba, M., Fröhlich, J. and Rodi, W. 2004*a* "On inflow boundary conditions for large eddy simulation of turbulent swirling jets". In *Proc. 21st Int. Congress of Theoretical and Applied Mechanics. Warsaw. Poland*.

García-Villalba, M., Fröhlich, J. and Rodi, W. 2004*b* "Unsteady phenomena in an unconfined annular swirling jet". In *Advances in Turbulence X* (eds. H. Andersson and P. Krogstad), pp. 515–518. Barcelona, Spain: CIMNE.

García-Villalba, M., Fröhlich, J. and Rodi, W. 2005 Large Eddy Simulation of the near field of a turbulent free annular swirling jet". In preparation.

Gupta, A.K., Lilley, D.G. and Syred, N. 1984 "Swirl Flows". Abacus Press.

Hillemanns, R. 1988 "Das Strömungs- und Reaktionsfeld sowie Stabilisierungeigenschaften von Drallflamen unter dem Einfluss der inneren Rezirkulationszone". PhD thesis, University of Karlsruhe.

Hinterberger, C. 2004 "Dreidimensionale und tiefengemittelte Large-Eddy-Simulation von Flachwasserströmungen". PhD thesis, University of Karlsruhe.

Lu, X., Wang, S., Sung, H.-G., Hsieh, S.-Y. and Yang, V. 2005 "Large Eddy Simulations of turbulent swirling flows injected into a dump chamber". *J. Fluid Mech.* **527**, pp. 171–195.

Lumley, J.L. 1978 "Computational modeling of turbulent flow". *Adv. Appl. Mech.* **18**, pp. 123–176.

Pierce, C. and Moin, P. 1998*a* "Method for generating equilibrium swirling inflow conditions". *AIAA J.* **36** (7), pp. 1325–1327.

Pierce, C. and Moin, P. 1998*b* "Large Eddy Simulation of a confined coaxial jet with swirl and heat release". AIAA paper 98-2892.

Tang, S. and Ko, N. 1994 "Experimental investigation of the structure interaction in an excited coaxial jet". *Experimental Thermal and Fluid Science* **8**, pp. 214–229.

Wang, P., Bai, X.S., Wessman, M. and Klingmann, J. 2004 "Large eddy simulation and experimental studies of a confined turbulent swirling flow". *Phys. Fluids* **16** (9), pp. 3306–3324.

Wang, S., Hsieh, S.-Y. and Yang, V. 2003 "An LES study of unsteady flow evolution in a swirl-stabilized injector with external excitations". In *Proc. Turbulence and Shear Flow Phenomena 3*, pp. 905–910.

Wegner, B., Kempf, A., Schneider, C., Sadiki, A., Dreizler, A., Janicka, J. and Schäfer, M. 2004 "Large eddy simulation of combustion processes under gas turbine conditions ". *Prog. Comp. Fluid Dyn.* **4**, pp. 257–263.

Wicker, R. and Eaton, J. 1994 "Near field of a coaxial jet with and without axial excitation". *AIAA Journal* **32** (3), pp. 542–546.